World Scientific
www.worldscientific.com

A NANOSTRUCTURED POLYMORPH OF μ-OXOBIS(PHTHALOCYANINATOIRON(III)) STUDIED BY ANGULAR AND ENERGY DISPERSIVE X-RAY DIFFRACTION

ROBERTO MATASSA*, PAOLO BALLIRANO†, MARIA PIA DONZELLO*,
CLAUDIO ERCOLANI*, CLAUDIA SADUN* and RUGGERO CAMINITI*,‡

*Dipartimento di Chimica, Università degli Studi di Roma "La Sapienza"
P.le A. Moro 5, 00185 Roma, Italy

†Dipartimento di Scienze della Terra, Università degli Studi di Roma "La Sapienza"
P.le A. Moro 5, 00185 Roma, Italy
‡r.caminiti@caspur.it

A new approach of X-ray diffraction was used to investigate the nanostructured μ-Oxo(2) polymorph of μ-oxo-bis(phthalocyaninatoiron(III)), [PcFe–O–FePc]. The packing of the dinuclear units was determined by the Rietveld method on Angular Dispersive X-ray Diffraction (ADXD) data, whereas the intramolecular geometry was optimized by Energy Dispersive X-ray Diffraction (EDXD) exploiting the peculiar strength of those techniques. The dimension of the nanoparticles was estimated from the Fourier transform of the EDXD experimental structural function.

Keywords: Dimer; phthalocyanine; nanocrystalline; μ-Oxo; X-ray diffraction; Rietveld refinement.

1. Introduction

Phthalocyanines are synthetic tetrapyrrolic macrocycles extensively investigated for several decades due to their interest for basic research and a number of practical applications.[1] Monomeric phthalocyanine units of formula [PcM] (Pc = phthalocyaninato dianion, $C_{32}H_{16}N_8^=$; M = bivalent metal ion) have a substantially planar molecular structure, entirely permeated by π-electron conjugation. As a result of their structural and electronic features, spontaneous tendency has been observed for [PcM] systems to generate intermolecular π–π interactions and to be cofacially assembled in the solid state with formation of different polymorphs (α, β, γ, etc.).[2] Similarly, tendency to aggregation has been widely seen in solution and dimers or higher forms of mutual interaction are often

evidenced depending on the solvent, concentration, and ambient conditions in general.[3]

Forced cofacial arrangement of Pc units can also take place in species known as sandwich-type systems of formula $[PcMPc]^m$ ($m = -1, 0, +1$),[4] or iodine-doped partially oxidized related materials,[5] in the metal–metal bonded dinuclear species [PcM–MPc],[6] and in the series of single-atom bridged dimers of formula [PcM–X–M′Pc] (M equal or different from M′), the most thoroughly studied being those with X = O, N, or C.[7] Among the few known μ-oxo-bridged dimers of formula [PcM–O–MPc],[7] the Fe(III)-containing species [PcFe^{III}–O–Fe^{III}Pc] was previously synthesized and shown to exist in two different polymorphs, named μ-Oxo(1) and μ-Oxo(2), based on UV-visible, IR and Mössbauer spectral measurements and magnetic

behavior.[8] These data were found to be consistent with a linear arrangement of the Fe–O–Fe bond system in μ-Oxo(2) (Chart 1(a)).[8a] This structural feature is also confirmed by the observed isomorphism of the polymorph with the related species [PcMn–O–MnPc] obtained by depyridination of the adduct [(py)PcMn–O–MnPc(py)] characterized by a linear N(Pc)–Mn–O–Mn–(Pc)N bond system as determined by X-ray work.[9] A bent Fe–O–Fe angle (Chart 1(b))[8b] was instead assigned to the polymorph μ-Oxo(1) and, from EXAFS measurements, Fe^{III}–N_p bond distances were established to be larger.[10]

The PcFe–O–FePc entity, according to single-crystal X-ray work, shows a linear Fe–O–Fe bond system in the complexes containing six-coordinated Fe(III), namely [(1-Meim)PcFe–O–FePc(1-Meim)][11] and the recently reported [(py)PcFe–O–FePc(THF)] (THF = tetrahydrofurane).[12] On the contrary, no direct information is available on the molecular structure and type of aggregation in the solid polymorph μ-Oxo(2), which contains five-coordinated Fe(III) centers. To our knowledge, there is only one similarly formulated species for which the structure has been unequivocally elucidated by single crystal X-ray

work, i.e., the Al(III) species [PcAl–O–AlPc].[13] Relevant features of the molecule are: (a) out-of-plane displacement of the five-coordinated Al^{III} ions towards the oxygen atom; (b) linear Al–O–Al bond system; and (c) eclipsed arrangement of the two Pc units. The energy dispersive X-ray diffraction technique (EDXD) has been successfully applied by us to the investigation of a number of phthalocyanine materials characterized by a short range order.[14]

This type of materials exhibit nanoscale local structures often originated by competing interactions within the materials. It is important to characterize these "nanostructures" but they are not, by their nature, long-range ordered and cannot be studied using conventional crystallographic methods.

This manuscript reports an application of a nonconventional X-ray diffraction method for determining the microstructural features of the nanocrystalline polymorph μ-Oxo(2) of μ-oxobis(phthalocyaninatoiron(III)), [(PcFe)$_2$O]. The need for a nonconventional crystallographic approach is related to the very large experimental peak broadening of the sample arising from the reduced dimensions of the grains.

In the present work, the EDXD technique has been complemented by the ADXD (angular dispersive X-ray diffraction technique), for obtaining an unequivocal definition of intra- and intermolecular contacts. A combination of these techniques will be proved as particularly suited for the investigation of the nanostructured material because of their complementary features. In fact, the ADXD is able to provide detailed information about molecular packing (i.e., long distances), whilst the EDXD gives reliable information on the molecular geometry because of the extended accessible q scattering parameter range. Moreover, the Radial Distribution Function (RDF), Fourier transform of the EDXD experimental data, supplies information on the dimension of the supramolecular organization of single nano-objects.
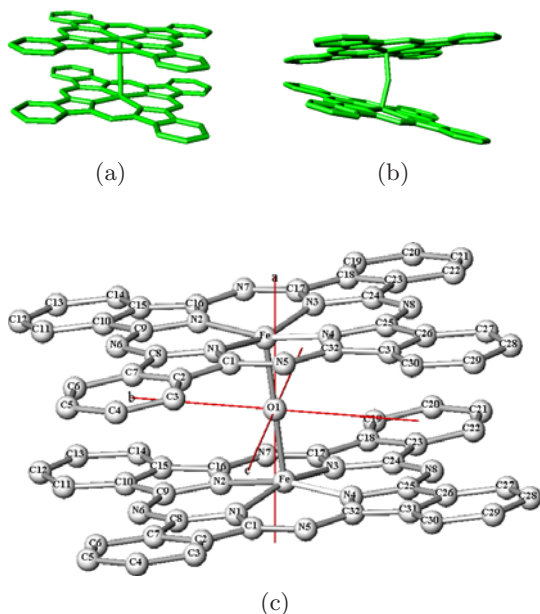
Chart 1. Structural models of the two known polymorphs of μ-oxobis(phthalocyaninatoiron(III)). (a) 3D view of the basic molecular structure of the μ-Oxo(2) polymorph formed by two cofacially arranged Pc units linked by a linear Fe–O–Fe bridge. (b) 3D view of the alternative polymorph μ-Oxo(1) formed by two tilted Pc units involving a bent Fe–O–Fe conformation. (c) Structural model showing the atomic numbering scheme for the μ-Oxo(2) polymorph.

2. Materials and Methods

2.1. *Synthesis of μ-oxobis (phthalocyaninatoiron(III)) (μ-Oxo(2) polymorph)*

The μ-Oxo(2) polymorph was prepared as described previously[8b] by bubbling dioxygen into a solution

of [PcFe] (334 mg, 0.59 mol) in concentrated H_2SO_4 (96%) for 50 min. Precipitation of the μ-oxo-bridged dimer was obtained by carefully pouring the brown H_2SO_4 solution into iced water so as to maintain the temperature below 25°C. The green solid precipitated was separated by centrifugation, washed several times with water until neutrality, then with acetone and brought to constant weight under vacuum (10^{-2} mmHg) (169 mg; yield 50%). Calculated for $C_{64}H_{32}Fe_2N_{16}O$: C, 66.68; H, 2.80; N, 19.44%. Found: C, 66.49; H, 2.66; N, 20.11%.

2.2. ADXD data collection and processing

X-ray powder diffraction data were collected on a parallel-beam Bruker AXS D8 Focus diffractometer, operating in Debye–Scherrer geometry equipped with Göbel mirrors on the incident beam and a Si(Li) Peltier-cooled solid state detector, using CuKα radiation. This configuration is especially suited for structural analysis because of the absence of preferred orientation. A powdered sample of μ-Oxo(2) was loaded inside a 0.5 mm diameter borosilicate glass capillary that was mounted and aligned on a standard goniometer head. Rietveld refinements were carried out using the GSAS[15] crystallographic suite of programs. Effective absorption measurements were carried out by collecting the intensity of the transmitted beam $I_t(E)$ through the sample and the intensity of the incident primary beam $I_0(E)$, both in direct transmission. The measured effective absorption was kept fixed throughout the refinements. Experimental details are reported in Table 1(a). Data were collected up to a maximum angular value of 60° 2θ because no further peaks were detected from a fast preliminary scan due to the large peak broadening arising from the very small crystallite size and the limited incident intensity of a conventional X-ray sealed tube. The asymmetry-modified pseudo-Voigt[16] was chosen as the peak profile function. Refined variables were GW (angle-independent) Gaussian, and LX ($(\cos\theta)^{-1}$-dependent) and LY ($\tan\theta$-dependent) Lorentzian and S/L, and H/L asymmetry parameters (constrained to be equal in magnitude). The background was fitted with a 16-terms Chebyshev polynomial of the first kind. Such a large number of terms were required to properly model the amorphous contribution of the

capillary. Cell parameters and positional parameters were subsequently refined allowing for peak position correction for sample displacement from the focusing circle. The geometry of the system was restrained using 185 soft constraints with a statistical weight associated to each observation equal to 10 (full list of soft constraints available from the authors upon request). This was done to avoid divergence or convergence toward false minima. U_{iso} displacement parameters were kept fixed. Miscellaneous data of the final refinement and cell parameters are reported in Table 1(b).

2.3. EDXD data collection and processing

A finely ground sample of μ-Oxo(2) (50–70 mg) was loaded on the sample holder.[17] Data were collected with a custom built X-ray energy scanning diffractometer.[18] The complete

Table 1. Experimental details and miscellaneous data of the Rietveld refinement of the μ-Oxo(2) polymorph of $[(PcFe)_2O]$.

(a) Experiment details	
Instrument	Bruker AXS D8Focus
X-ray tube	Cu at 40 kV and 40 mA
	(CuKα_1 = 0.1540598 nm)
Incident beam optic	Multilayer X-ray mirrors
Sample mount	Rotating capillary (30 rpm)
Soller slits	2 (2.3° divergence)
Div. and antidiv. slits	1 mm
Detector slit	0.2 mm (0.10°)
Detector	SSD Si(Li) SolX
2θ range (°)	3–60 (2851 data points)
Step size (°)	0.02
Counting time (s)	30

(b) Miscellaneous data of the refinement			
Space group	$P\bar{1}$	R_{Bragg}	0.021
a (nm)	0.7475 (31)	DWd	1.665
b (nm)	1.2802 (18)	Reduced χ^2	1.486
c (nm)	1.2726 (14)	Soft constr.	5.2
		contr. to χ^2 (%)	
α (deg)	88.69 (8)	Refined	152
		parameters	
β (deg)	96.52 (19)	GU	43520 (430)
γ (deg)	89.64 (10)	GV	$-$5665 (1144)
V (nm^3)	120.95 (13)	GW	279 (58)
ρ_{calc} (g/cm^3)	1.538	LX	29 (6)
R_p	0.032	LY	0
wR_p	0.045	S/L = H/L	0.0277 (3)

experimental scattering parameter range, $q = 2$–$170\,\mathrm{nm}^{-1}$ was explored by performing several measurements in correspondence with a set of scattering angles, θ, at $26.0°$, $15.5°$, $8.0°$, $3.5°$, $2.0°$, $1.0°$, and $0.5°$ using the relation $q = 4\pi\sin\vartheta/\lambda = EC\sin\vartheta$, where q is expressed in $[\mathrm{nm}^{-1}]$, λ in $[\mathrm{nm}]$; the utilized energy range is $E_{\min} = 13.5\,\mathrm{keV}$ and $E_{\max} = 38.2\,\mathrm{keV}$ and the value of the constant C is $10.14\,[(\mathrm{keV}*\mathrm{nm})^{-1}]$. The experimental static structure function SF, the experimental radial distribution $D(r)$ and the form $D_{\mathrm{iff}}(r) = D(r) - 4\pi r^2\rho_0$ were obtained as detailed previously (Figs. 1(a) and 1(b)).[19] Theoretical peak shapes were calculated by Fourier transforming the theoretical structure function, calculated by the Debye equation for the pair interactions of the theoretical models proposed:

$$i_{mn}(q) = \sum_{m\neq n}^{N} f_m(q)f_n(q)\left(\frac{\sin(r_{mn}q)}{r_{mn}q}\right)\exp\left(-\frac{1}{2}\sigma_{mn}^2 q^2\right),$$
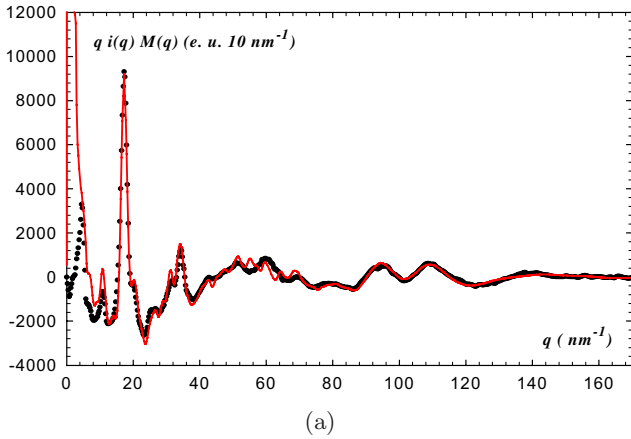
(a)
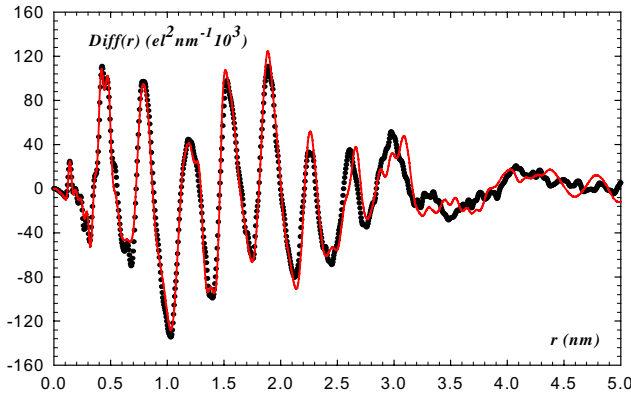
(b)

Fig. 1.   Structural analysis of the μ-Oxo(2) polymorph by the EDXD technique. (a) Experimental structural SF (dots) and theoretical curve (solid line) calculated for 36 unit cells, and (b) the corresponding Fourier transform Diff(r).

Table 2.   Final values of the adjusted rms σ for the model used.

Distance range (nm)	σ
$0.00 < r \leq 0.19$	0.054
$0.19 < r \leq 0.50$	0.102
$0.50 < r$	0.270

where r_{mn} corresponds to the distance between m and n atoms and σ_{mn} is the root-mean-square (rms) in the interatomic distance. The number of parameters was reduced by taking the same σ value for distances falling within predefined ranges r_{mn}, instead of using a different σ_{mn} value for each distance. The distance ranges of the interatomic interactions and the associated rms σ were determined and the values are reported in Table 2.

For calculating the best agreement between experimental data and theoretical peaks, we used the formula:

$$R_{\mathrm{Hamilton}} = \sqrt{\frac{\sum_{i=1}^{m}\|F^e(q_i)| - |F^c(q_i)\|^2}{\sum_{i=1}^{m}|F^c(q_i)|^2}},$$

where the ith index runs over the m experimental points and the e and c labels of $F(q_i)$ refer to the experimental and calculated structural functions.

3.   Results and Discussion

Data by the EDXD technique were collected in the $2 < q < 170\,\mathrm{nm}^{-1}$ range (Fig. 1(a)), whereas those from the ADXD technique were obtained in the $2 < q < 40\,\mathrm{nm}^{-1}$ range (Fig. 2). In the common range, the main experimental peaks of the two diffraction patterns are located in the same positions. The EDXD experimental structure function (SF) shows two further broad peaks of low intensity located at about 51.0 and $59.7\,\mathrm{nm}^{-1}$ followed by two large oscillations at higher q values, related to intramolecular contacts.

The Fourier transform of the SF, i.e., the radial distribution function in the Diff(r)-form, is reported in Fig. 1(b) in the range 0–5 nm. The Diff(r) provides direct information in real space on the
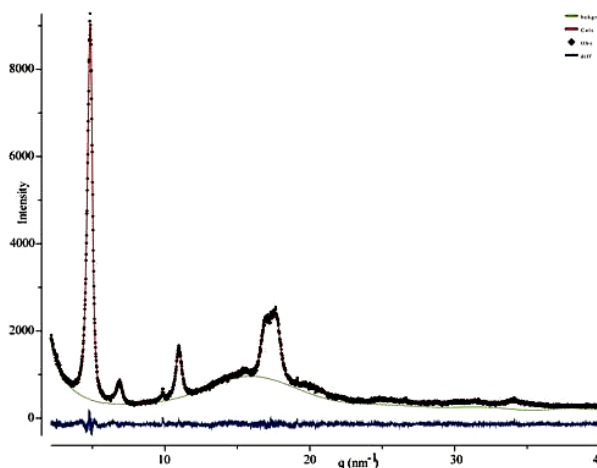
Fig. 2. Observed, calculated and difference plots of the Rietveld refinement of the μ-Oxo(2) polymorph of $[(\text{PcFe})_2\text{O}]$ from ADXD data. Vertical marks refer to the position of calculated Bragg reflections.

inter- and intramolecular contacts. Owing to the large dimensions of the molecular unit, the peaks in the range 0.1–1.7 nm contain both intra- and interunit contributions, while the peaks at higher r values (> 1.2 nm) are due to interunit interactions only. The intensity of the peaks at values of $r \gtrsim 3.5$ nm becomes very small, suggesting that no further regular structure is present.

For the detailed interpretation of the structural features of the dinuclear μ-Oxo(2) polymorph, it was particularly useful to refer to the structure of the similarly formulated Al(III) species $[(\text{PcAl})_2\text{O}]$,[13] which shows an out-of-plane displacement of the five-coordinate Al(III) atoms by 0.046 nm towards the bridging O atom and a linear Al–O–Al bond system (Al–O $= 0.168$ nm; Al–$N_p = 0.196$ nm). Quite peculiar is the eclipsed arrangement of the two Pc units, apparently not requested by steric hindrance due to the long Pc–Pc average distance (0.427 nm). Working within the hypothesis of an occurring isomorphism between the Al(III) species and μ-Oxo(2), the ADXD study on μ-Oxo(2) was performed by using the $[(\text{PcAl})_2\text{O}]$ structural parameters. The starting unit cell parameters for this Al(III) species are $a = 0.769$ (4) nm, $b = 1.252$ (3) nm, $c = 1.271$ (3) nm, $\alpha = 91.03$ (2)°, $\beta = 94.54$ (2)°, $\gamma = 90.37$ (2)°, $Z = 1$ and triclinic space group $P\bar{1}$.

A first Rietveld refinement of μ-Oxo(2) was carried out without optimizing the fractional coordinates. In fact, because of the very large peak broadening arising from the reduced dimensions of

the grains, it was only possible to refine the cell parameters, in the absence of structural constraints. Despite the impossibility to obtain a satisfactory fit between the experimental and calculated patterns, especially for the broad peaks at $17.2 \, \text{nm}^{-1}$, the isomorphism between $[(\text{PcAl})_2\text{O}]$ and μ-Oxo(2) was easily proved. The ADXD structural data of $[(\text{PcAl})_2\text{O}]$ (modified with the cell parameters refined by the Rietveld method) were subsequently utilized to build a theoretical structural function, and a theoretical radial distribution function, to be compared with the EDXD experimental data. Moreover, the agreement between the experimental and the theoretical functions were found not acceptable in the range of the intramolecular interactions between $40 \, \text{nm}^{-1}$ and $170 \, \text{nm}^{-1}$.

Based on these results and pointing to a better agreement between experimental and calculated data, an iterative fitting process between the two techniques was carried out. The structural parameters obtained from the refinement of the ADXD data were used as starting point for the EDXD fitting. Subsequently, the refined structural parameters from EDXD data were employed for a new refinement of the ADXD data and so on.

Comparison of the theoretical structural function with the EDXD experimental one in the range between $40–170 \, \text{nm}^{-1}$, clearly suggested the need for an optimization of the structural parameters of μ-Oxo(2).

The local geometry of the dinuclear unit, i.e., the Fe–N and Fe–O bond lengths, and the overall geometry of the molecular framework within each Pc unit were fitted unconstrained. Different structural geometrical features were tested, i.e., nonplanarity of the molecular units, interunit contacts within the dimer, molecular rotation and tilting.

Soft constraints on bond distances, suggested by the fitted geometry on the EDXD data, were used for a second refinement of the ADXD data. In this case, the refinement smoothly converged to agreement indices $R_p = 0.032$, $wR_p = 0.045$, $\chi^2 = 1.486$, and $R_{\text{Bragg}} = 0.021$ (statistical indicators as described in Ref. 20. Final experimental, calculated, and difference Rietveld plots are reported in Fig. 2.

The second refinement of the structural parameters of μ-Oxo(2) obtained by the ADXD method was used to calculate again the theoretical SF and to evaluate the agreement with the EDXD experimental structural function. The R_{Hamilton} estimate error was 23.34%. An optimization

procedure was reiterated because the theoretical structural model showed that the Pc units of the μ-oxo dimer were affected by an unrealistically anomalous over distortion. As a result, the molecular distortions of the μ-oxo dimer disappear, providing a structural geometry similar to that of the μ-oxo complex [(PcAl)$_2$O]. The atomic Cartesian coordinates corresponding to this dimeric model are reported in Table 3, corresponding to Chart 1(c).

The RDF analysis in the Diff(r)-form is crucial to solve the structure of nanocrystalline materials by comparison to several models tested until a good match is achieved. The best agreement between the experimental data and theoretical Diff(r) for μ-Oxo(2) was found by considering a block of 36 unit cells. The cluster consists of four dimers stacked along the a-axis as required by the presence of the main experimental peak at $17.2\,\text{nm}^{-1}$ and nine molecular columns arranged along the b- and c-axes as a rational consequence of the presence of the peaks at 4.8 and $10.8\,\text{nm}^{-1}$. The final theoretical structural function was found in good agreement with the experimental data with a R_{Hamilton} estimate error of 17.24%, as shown in Figs. 3(a) and 3(b).

The metal ion in the μ-Oxo(2) polymorph forms Fe^{III}–N_p bonds with a distance of 0.191 nm, and is displaced out of the Pc plane by 0.021 nm towards the bridging oxygen atom. The Fe–O bond distance is 0.175 nm and the angle for the Fe^{III}–O–Fe^{III} fragment is 180°. The Pc units are substantially planar and the interplanar distance is 0.392 nm. The Fe^{III}–N_p distance is only slightly shorter than the mean value (0.193 nm) of the four Fe^{II}–N_p bond lengths in the monomeric iron(II) phthalocyanine, [PcFe].[21] This is likely to be due to the +3 charge residing on the metal ion. It should be also noted that in the species [PcFeCl]$_2$I$_2$, having the two PcFeCl fragments held together by the central and symmetrically residing I$_2$ molecule, the Fe(III) centers form slightly longer Fe^{III}–N_p bond distances (0.1945 (3) nm) and are pulled out of the average Pc plane by 0.030 nm due to the presence of the apical Cl atoms.[22]

The ADXD technique supplies suitable information on the spatial distribution of the μ-Oxo(2) units by Rietveld refinement. It is triclinic, space group $P\bar{1}$, cell parameters a = 0.7475 (33) nm, b = 1.280 (18) nm, c = 1.273 (14) nm, α = 88.69 (8)°, β = 96.53 (19)°, γ = 89.64 (10)° and Z = 1. The eclipsed dimers are stacked along the a-axis,

Table 3.   Final positional parameters and isotropic thermal parameters of nonhydrogen.

Atoms	x	y	z	U_{iso}
Fe	0.2305 (6)	0.0182 (11)	− 0.0062 (14)	0.020
O1	0.0	0.0	0.0	0.030
N1	0.2989 (19)	− 0.1138 (14)	0.0614 (16)	0.027
N2	0.2690 (27)	0.0840 (11)	0.1285 (16)	0.027
N3	0.1986 (24)	0.1532 (11)	− 0.0750 (15)	0.027
N4	0.2287 (32)	− 0.0451 (14)	− 0.1416 (15)	0.027
N5	0.336 (4)	− 0.0672 (14)	0.2453 (17)	0.027
N6	0.210 (5)	0.2647 (10)	0.0770 (16)	0.027
N7	0.160 (5)	0.1057 (14)	− 0.2583 (15)	0.027
N8	0.285 (5)	− 0.2262 (16)	− 0.0899 (17)	0.027
C1	0.343 (8)	− 0.1317 (16)	0.1676 (18)	0.035
C2	0.293 (8)	0.0332 (14)	0.2251 (16)	0.035
C3	0.268 (7)	0.1056 (13)	0.3083 (17)	0.035
C4	0.293 (10)	0.0906 (16)	0.4181 (17)	0.035
C5	0.356 (13)	0.1782 (25)	0.4760 (22)	0.035
C6	0.366 (14)	0.2777 (25)	0.4254 (23)	0.035
C7	0.308 (15)	0.2932 (15)	0.3177 (17)	0.035
C8	0.256 (6)	0.2041 (13)	0.2600 (16)	0.035
C9	0.236 (6)	0.1870 (11)	0.1465 (16)	0.035
C10	0.166 (4)	0.2444 (11)	− 0.0254 (15)	0.035
C11	0.126 (4)	0.3273 (12)	− 0.1049 (16)	0.035
C12	0.187 (8)	0.4306 (17)	− 0.1052 (21)	0.035
C13	0.184 (7)	0.4805 (24)	− 0.2058 (24)	0.035
C14	0.087 (9)	0.4357 (28)	− 0.2965 (21)	0.035
C15	0.023 (7)	0.3335 (18)	− 0.2925 (17)	0.035
C16	0.072 (5)	0.2755 (15)	− 0.1984 (16)	0.035
C17	0.147 (6)	0.1705 (14)	− 0.1810 (14)	0.035
C18	0.192 (9)	0.0040 (16)	− 0.2383 (15)	0.035
C19	0.215 (9)	− 0.0696 (14)	− 0.3213 (16)	0.035
C20	0.188 (14)	− 0.0567 (15)	− 0.4313 (16)	0.035
C21	0.154 (20)	− 0.1478 (26)	− 0.4904 (21)	0.035
C22	0.157 (21)	− 0.2477 (22)	− 0.4391 (20)	0.035
C23	0.194 (20)	− 0.2599 (17)	− 0.3294 (21)	0.035
C24	0.224 (9)	− 0.1679 (13)	− 0.2721 (16)	0.035
C25	0.245 (11)	− 0.1497 (15)	− 0.1590 (16)	0.035
C26	0.298 (5)	− 0.2085 (14)	0.0135 (17)	0.035
C27	0.358 (8)	− 0.2898 (13)	0.0916 (21)	0.035
C28	0.370 (9)	− 0.3983 (12)	0.0833 (22)	0.035
C29	0.420 (9)	− 0.4555 (12)	0.1783 (23)	0.035
C30	0.493 (10)	− 0.4028 (15)	0.2705 (27)	0.035
C31	0.472 (10)	− 0.2948 (16)	0.2789 (25)	0.035
C32	0.406 (7)	− 0.2393 (13)	0.1861 (21)	0.035

showing a cofacial aggregation and separated by a distance of 0.352 nm.

These structural parameter values have been utilized to achieve the theoretical radial distribution function Diff(r) to be compared with the EDXD experimental one. The model has recognized a dimeric cluster constituted of nine dimeric columns of four dimers extended along the b- and c-axes, having a parallelepiped shape of about

(a)

(b)
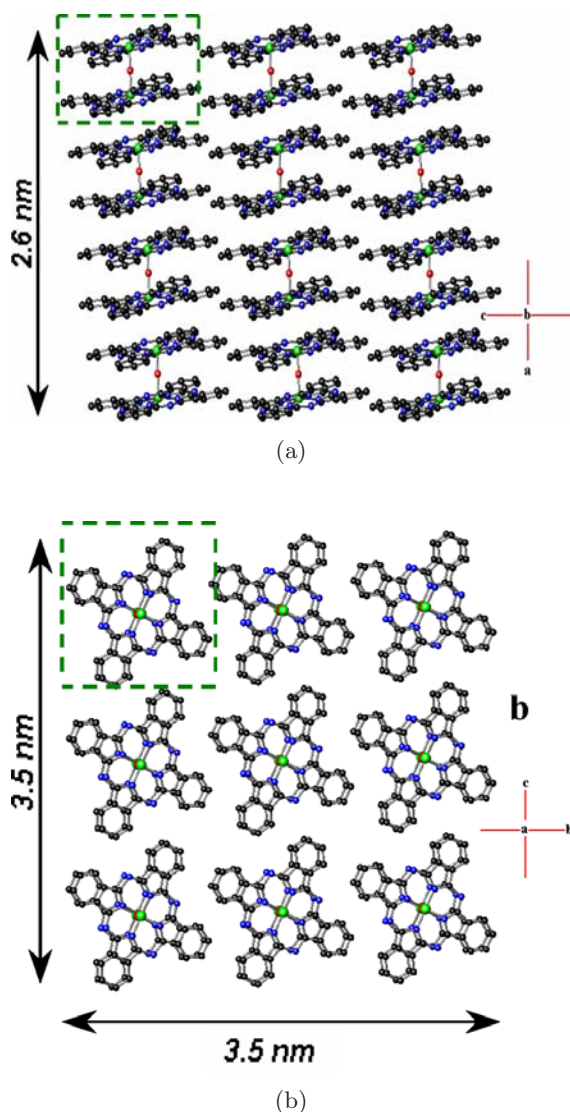
Fig. 3. Molecular arrangement in the nanocrystalline μ-Oxo(2) calculated by EDXD method, assuming the crystal parameters obtained by ADXD method. (a) Stacking of the dinuclear units as seen along [010]. (b) Projection of the structure along [100]. A single unit cell is indicated by the - - - line.

$3.5 \times 3.5 \times 2.6$ nm dimension, as shown in Figs. 3(a) and 3(b).

4. Conclusions

In this paper, we have performed the structural identification of the μ-Oxo(2) polymorph of $[PcFe]_2O$ by combining two different X-ray diffraction techniques. They provide indisputable evidence of the nanostructure of powered material. In a combined utilization, the ADXD and EDXD techniques proved that the μ-Oxo(2) polymorph is isomorphous with $[(PcAl)_2O]$. On the contrary, because of their constitutional limits, they could not

be as well informative if utilized separately. In fact, the ADXD exploration only able to provide information regarding the packing of the dinuclear units, but the resulting dimeric structure was strongly distorted due to the limited portion of reciprocal-space accessible by this technique. Instead more accurate information on the intra-unit contacts and on the size of the nano-objects was extracted by the theoretical Diff(r) analysis of the EDXD method. This is why these techniques may be considered as complementary in the case of structural analysis of nanocompounds.

Acknowledgment

References

1. K. M. Kadish, K. M. Smith and R. Guilard (eds.), *The Porphyrin Handbook*, Vols. 15–20 (Academics Press, New York, 2003).
2. M. K. Engel, *The Porphyrin Handbook*, Vol. 20, eds. K. M. Kadish, K. M. Smith and R. Guilard (Academic Press, New York, 2003), Chapter 122, p. 1.
3. A. W. Snow, *The Porphyrin Handbook*, Vol. 17, eds. K. M. Kadish, K. M. Smith and R. Guilard (Academic Press, New York, 2003), Chapter 109, p. 130.
4. E. M. Bauer, M. P. Donzello, C. Ercolani, E. Masetti, S. Panero, G. Ricciardi, A. Rosa, A. Chiesi-Villa and C. Rizzoli, *Inorg. Chem.* **42**, 283 (2003); H. Hückstädt, A. Tutas, M. Goldner, M. Cornelissen and H. Homborg, *Zeit. Anorg. Allg. Chem.* **627**, 485 (2001).
5. J. Janczak, *Inorg. Chem.* **42**, 3549 (2003).
6. C. Ercolani, *J. Porphyrins Phthalocyanines* **4**, 340 (2000); M. Göldner, H. Hückstädt, K. S. Murray, B. Moubaraki and H. Homborg, *Zeit. Anorg. Allg. Chem.* **624**, 288 (1998).
7. B. Floris, M. P. Donzello and C. Ercolani, *The Porphyrin Handbook*, Vol. 18, eds. K. M. Kadish, K. M. Smith and R. Guilard (Academic Press, New York, 2003), Chapter 112, p. 1.
8. (a) C. Ercolani, M. Gardini, F. Monacelli, G. Pennesi and G. Rossi, *Inorg. Chem.* **22**, 2584 (1983); (b) C. Ercolani, M. Gardini, K. S. Murray, G. Pennesi and G. Rossi, *Inorg. Chem.* **25**, 3972 (1986).
9. L. H. Vogt, Jr., A. Zalkin and D. H. Templeton, *Inorg. Chem.* **6**, 1725 (1967).
10. J. K. Choi, G. Kwag and S. Kim, *J. Electroanal. Chem.* **508**, 105 (2001).

11. C. Ercolani, F. Monacelli, S. Dzugan, V. L. Goedken, G. Pennesi and G. Rossi, *J. Chem. Soc., Dalton Trans.* **5**, 1309 (1991).

12. M.-J. Lin, J.-D. Wang, N.-S. Chen and J.-L. Huang, *Inorg. Chem. Commun.* **8**, 900 (2005).

13. K. J. Wynne, *Inorg. Chem.* **24**, 1339 (1985).

14. R. Caminiti, A. Capobianchi, P. Marovino, A. M. Paletti, G. Padeletti, T. Pennesi and G. Rossi, *Thin Solid Films* **382**, 70 (2001); R. Caminiti, M. P. Donzello, C. Ercolani and C. Sadun, *Inorg. Chem.* **38**, 3027 (1999); R. Caminiti, M. P. Donzello, C. Ercolani and C. Sadun, *Inorg. Chem.* **37**, 4210 (1998).

15. A. C. Larson and R. B. Von Dreele, GSAS general structure analysis system, LAUR 86-748, Los Alamos National Laboratory, The Regents of the University of California (1985).

16. L. W. Finger, D. E. Cox and A. P. Jephcoat, *J. Appl. Cryst.* **27**, 892 (1994).

17. R. Caminiti, C. Sadun, V. Rossi Alberini, F. Colloco and R. Felici, *XXV Italian Congress on Physical Chemistry*, Cagliari, Italy (1991).

18. R. Caminiti, C. Sadun, V. Rossi Alberini, F. Colloco and R. Felici, Patent No. RM/93 01261484, 23 June 1993.

19. M. Carbone, R. Caminiti and C. Sadun, *Trends in Chem. Phys. Res.* **11**, 75 (2004).

20. R. A. Young, Introduction to the Rietveld method, *The Rietveld Method*, ed. R. A. Young (Oxford Science, Oxford, 1993), pp. 1–38.

21. J. F. Kirner, W. Dow and W. R. Scheidt, *Inorg. Chem.* **15**, 1685 (1976).

22. S. M. Palmer, J. L. Stanton, N. K. Jaggi, B. M. Hoffman, J. A. Ibers and L. H. Schwartz, *Inorg. Chem.* **24**, 2040 (1985).